CONFORMAL MAPPING FOR THE EFFICIENT MFS SOLUTION OF DIRICHLET BOUNDARY VALUE PROBLEMS*

ANDREAS KARAGEORGHIS† AND YIORGOS–SOKRATIS SMYRLIS†

ABSTRACT. In this work, we use conformal mapping to transform harmonic Dirichlet problems that are defined in simply–connected domains into harmonic Dirichlet problems that are defined in the unit disk. We then solve the resulting harmonic Dirichlet problems efficiently using the Method of Fundamental Solutions (MFS) in conjunction with Fast Fourier Transforms (FFTs). This technique is extended to harmonic Dirichlet problems in doubly–connected domains which are now mapped onto annular domains. The solution of the resulting harmonic Dirichlet problems can be carried out equally efficiently using the MFS with FFTs. Several numerical examples are presented.

1. INTRODUCTION

In Trefftz methods [3, 11], the solution of a boundary value problem is approximated by a linear combination of special solutions of the governing equation of the problem in question. One such method is the Method of Fundamental Solutions (MFS) in which the solution is approximated by a linear combination of fundamental solutions of the operator of the governing equation, with singularities (sources) located outside the domain of the problem. The MFS has become increasingly popular in recent years primarily due to the simplicity of its implementation. One of the fundamental questions in the application of the MFS is the positioning of the sources. One way of dealing with this problem is to let the coordinates of the sources be free, and determine their locations by solving a non–linear least–squares problem [5, 15]. However, this approach could be costly and has some drawbacks such as the possibility of the existence of several minima in the non-linear least-squares minimization process. Alternatively, one may use the version of the MFS where the sources are preassigned (fixed) [6] on a pseudo-boundary surrounding, and usually similar in shape to, the boundary of the problem in question ([7]). The solution of Dirichlet harmonic problems in disks, when using the latter approach, has been the subject of several studies [9, 10, 20, 21, 22]. In these, convergence analyses and error estimates are presented, and efficient FFT-based methods are proposed. Similar results for Dirichlet harmonic problems in annular domains may be found in [27]. Both the theoretical and implementational aspects of the MFS is these cases are well understood. Further, the conditioning of the coefficient matrices arising in the MFS discretization is known to be poor. This ill–conditioning is exacerbated when the domain of the problem under consideration is non–smooth, when the number of degrees of freedom becomes large, and when the distance of the pseudo–boundary from the boundary is large. These implementational difficulties may be alleviated in the case of domains with rotational symmetry. (See [20, Section 4.7].) In the general case of domains without rotational symmetry, the challenge becomes the determination of the distance of the pseudo-boundary from the boundary. One way of overcoming this difficulty, proposed in [25], is to solve the boundary value problem with the MFS for a range of values of the distance of the pseudo–boundary from the boundary and for each distance

*Technical Report TR–27–2007, Department of Mathematics and Statistics, University of Cyprus, October 2007.

†This work was supported by University of Cyprus grant #8037-3/312-21005.

‡*Typeface* Palatino, Mathpazo– *System* LaTeX2$_\varepsilon$.

Date: October 29, 2007.

2000 *Mathematics Subject Classification.* Primary 30C20, 35E05, 65N35; Secondary 30C30, 65N38.

Key words and phrases. Method of fundamental solutions, Laplace equation, conformal mapping, circulant matrices.

find the maximum error in the satisfaction of the boundary conditions on a fixed set of boundary points (different from the MFS collocation points). The optimal value of this distance is the one for which the maximum error is minimal. This approach, however, requires the solution of a sequence of problems and could be potentially expensive. In view of the fact that Dirichlet boundary value problems on disks and annuli may be solved efficiently, in this work we shall transform a given problem in a simply–connected (resp. doubly–connected) domain into a problem in the unit disk (resp. an annulus) using conformal mappings and then to solve the transformed problem efficiently. In this approach, it is interesting to observe that when the conformal mapping opens up an angle, then a singularity is introduced in the image point of the transformed domain. On the other hand, singularities due, for example, to re–entrant corners can be removed by conformal transformations onto the disk.

The purpose of this paper is to show, apparently for the first time, how conformal mappings can be used to transform harmonic Dirichlet problems in simply– and doubly–connected domains onto problems in the unit disk and appropriate annuli, respectively, where they can be solved efficiently using FFT–based matrix decomposition algorithms. Also, in this work we illustrate some of the potential difficulties associated with this technique, such as the introduction of boundary singularities in the transformed problems.

We consider the solution of Laplace's equation in the complex $z = x + \mathrm{i}y-$plane,

$$\Delta u = 0 \quad \text{in} \quad \Omega, \tag{1.1a}$$

subject to the Dirichlet boundary condition

$$u = f(x, y) \quad \text{on} \quad \partial\Omega, \tag{1.1b}$$

where the domain Ω is simply–connected. The idea is to use the conformal mapping $\mathcal{F}$ to transform problem (1.1) into the boundary value problem in the complex $w = \xi + \mathrm{i}\eta-$plane,

$$\begin{cases} \Delta\tilde{u} = 0 & \text{in} \quad \widetilde{\Omega}, \\ \tilde{u} = \tilde{f}(\xi, \eta) & \text{on} \quad \partial\widetilde{\Omega}, \end{cases} \tag{1.2}$$

where $\widetilde{\Omega}$ is now the unit disk. If $\xi + \mathrm{i}\eta = x(\xi, \eta) + \mathrm{i}y(\xi, \eta)$ is the image of $x + \mathrm{i}y$ under $\mathcal{F}$, then $\tilde{u}(\xi, \eta) = u(x, y)$, and in particular, $\tilde{f}(\xi, \eta) = f(x, y)$. Boundary value problem (1.2) can be solved efficiently with the MFS using the techniques developed in [21, 22, 27].

The paper is organized as follows. In Section 2, we present several examples of problems in simply–connected domains which are mapped onto problems in the unit disk. In Section 3, we describe the efficient implementation of the MFS for the solution of harmonic Dirichlet problems in the unit disk. Numerical results for a number of examples are presented in Section 4. In Section 5, the techniques presented in sections 2–3 are extended to the case of doubly–connected domains. Finally, in Section 6, we provide some concluding remarks.

2. CONFORMAL MAPPINGS

The existence of conformal mappings for simply-connected domains is guaranteed from the *Riemann mapping theorem* (see e.g.,[29]) which states that *If Ω is a simply–connected domain, other that $\mathbb{C}$, and if $z_0 \in \Omega$, then there exists a unique conformal map $\mathcal{F}$ of Ω onto the unit disk so that $\mathcal{F}(z_0) = 0$ and $\mathcal{F}'(z_0) > 0$.* This mapping may be continuously extended from the boundary of Ω to the unit circle, if the former is a Jordan curve. (Carathéodory–Osgood Theorem [18].)

2.1. **Exterior of an ellipse.** We consider (1.1) in the complex plane when Ω is the exterior of an ellipse. More specifically, Ω is the exterior of the ellipse with major semi-axis $a = \cosh\alpha$ and minor semi-axis $b = \sinh\alpha$ in the complex $z-$plane. We know that the transformation [23]

$$z = \frac{1}{2}\left(w\,\mathrm{e}^{-\alpha} + w^{-1}\,\mathrm{e}^{\alpha}\right), \tag{2.1}$$

maps the interior of the unit disk to the domain Ω of problem (1.1). The inverse of transformation (2.1) is given by

$$w = \mathrm{e}^{\alpha}\left(z - \sqrt{z^2-1}\right), \tag{2.2}$$

and maps the domain Ω ($z-$plane) onto the interior of the unit disk ($w-$plane). Therefore, via transformation (2.2) the boundary value problem (1.1) in the $z-$plane with Ω the exterior of an ellipse is mapped onto problem (1.2) in the unit disk. The correspondence between the two domains is shown in Figure 1.

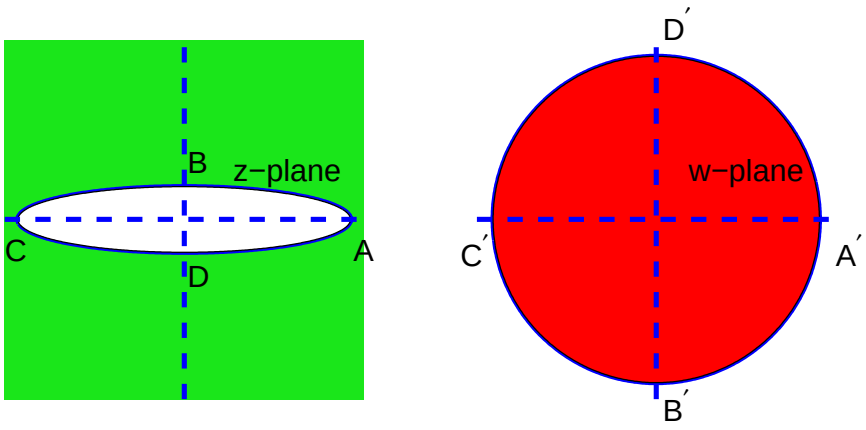

FIGURE 1. Conformal mappings from exterior of ellipse to disk

2.2. **Interior of an ellipse.** We next consider problem (1.1) in the complex plane when Ω is the interior of an elliptical domain, namely the interior of the ellipse with major semi-axis $a > 1$ and minor semi-axis $b = 1$ in the $z-$complex plane. The transformation ([16], page 296, see also [17])

$$w = \sqrt{k}\,\mathrm{sn}\left(\frac{2K(k)}{\pi}\sin^{-1}\left(\frac{z}{\sqrt{a^2-1}}\right), k\right), \tag{2.3}$$

maps the interior of the ellipse Ω of problem (1.1) onto the interior of the unit disk. In the above, sn is the Jacobian elliptic sine and $K(k)$ denotes the complete elliptic integral of the first kind with modulus k. The inverse of transformation (2.3) is given by

$$z = \sqrt{a^2-1}\,\sin\left(\frac{\pi}{2K(k)}\int_0^{\frac{w}{\sqrt{k}}}\frac{dt}{\sqrt{(1-t^2)(1-k^2t^2)}}\right),$$

and maps the unit disk ($w-$plane) onto Ω ($z-$plane). Thus, via transformation (2.3) the boundary value problem (1.1) in the interior of the ellipse in the $z-$plane is mapped onto problem 1.2 in the unit disk. The correspondence between the two domains is shown in Figure 2. It should be noted that the modulud k satisfies

$$\frac{K(k')}{K(k)} = \frac{2}{\pi}\sinh^{-1}\left(\frac{2a}{a^2-1}\right), \tag{2.4}$$

where $k' = \sqrt{1-k^2}$.

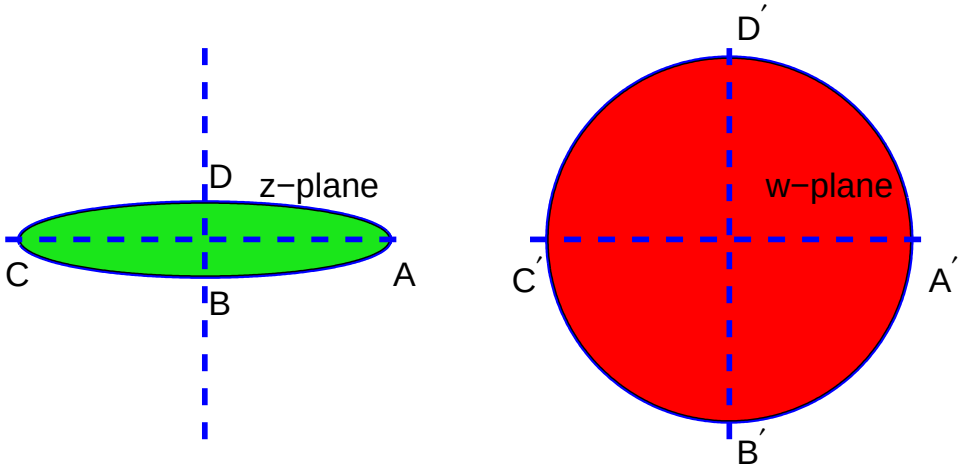

FIGURE 2. Conformal mappings from interior of ellipse to disk.

2.3. **Cardioid.** We next consider problem (1.1) in the complex plane when Ω is the interior of a cardioid, defined parametrically in polar coordinates by $r = 2a^2(1+\cos\theta)$ in the complex $z-$plane. The cardioid is mapped onto the interior of a disk of radius a with centre $v = a$ in the $v-$plane, via the transformation [23]

$$v = z^{1/2}. \tag{2.5}$$

The inverse mapping is given by

$$z = v^2.$$

This disk is subsequently mapped onto the unit disk via

$$w = \frac{1}{a}(v-a), \tag{2.6}$$

while the inverse mapping is given by

$$v = aw + a.$$

Thus, via transformation (2.5) boundary value problem (1.1) in the interior of the cardioid in the $z-$plane is mapped onto a problem in a disk with centre $v = a$ and radius a in the $v-$plane. Subsequently, this problem is mapped onto problem 1.2 in the unit disk in the $w-$plane via transformation (2.6). The correspondence between the three domains is shown in Figure 3.

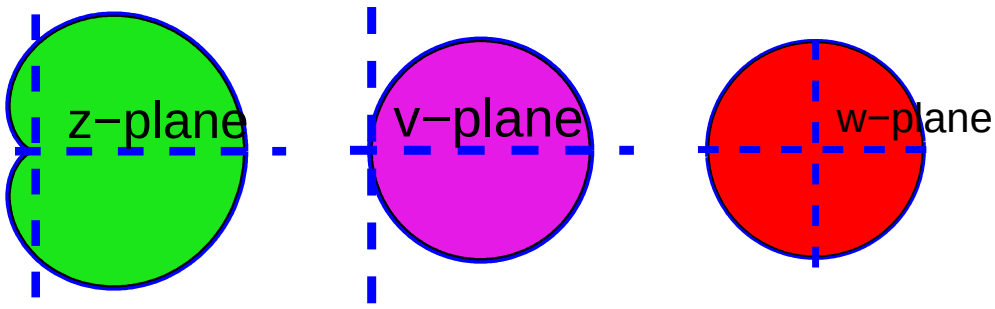

FIGURE 3. Conformal mappings from interior of cardioid to disk.

z	$-K+\mathrm{i}K'$	$-K$	0	K	$K+\mathrm{i}K'$	$\mathrm{i}K'$
v	$-k^{-1}$	-1	0	1	k^{-1}	∞
w	$\mathrm{e}^{2\mathrm{i}\tan^{-1}k}$	i	-1	$-\mathrm{i}$	$\mathrm{e}^{-2\mathrm{i}\tan^{-1}k}$	1

TABLE 1. Correspondence of points in $z-$, $v-$ and $w-$planes for rectangle.

z	A	B	C
v	0	1	∞
w	-1	$-\mathrm{i}$	1

TABLE 2. Correspondence of points in $z-$, $v-$ and $w-$planes for triangle.

2.4. **Rectangular domain.** We now consider problem (1.1) in the complex $z-$plane, in the case where Ω is a rectangle with corners $-K, K, K+\mathrm{i}K', -K+\mathrm{i}K'$, where K and K' are the complete elliptic integrals of the first kind with moduli $k<1$ and $k'=\sqrt{1-k^2}$, respectively. The problem is first mapped onto the upper half plane of the $v-$plane via the transformation given by the Jacobian elliptic function [16]

$$v = \mathrm{sn}\, z.$$

The inverse mapping is given by the incomplete elliptic integral of the first kind [16]

$$z = \int_0^v \frac{dv}{\sqrt{(1-v^2)\,(1-k^2v^2)}} = \mathrm{sn}^{-1}(v,k). \tag{2.7}$$

In (2.7), the modulus k depends on the ratio K'/K. For $0.3 \le K'/K \le 3$, the corresponding values of k may be found in [1], Table 17.3. The correspondence of the various points of the boundary $\partial\Omega$ of the rectangle and points on the real line are given in Table 1 [16]. From the upper half–plane in the $v-$plane onto the unit disk in the $w-$plane, we use the transformation

$$w = \frac{v-\mathrm{i}}{v+\mathrm{i}} \tag{2.8}$$

which has the inverse transformation

$$v = \mathrm{i}\,\frac{1+w}{1-w}. \tag{2.9}$$

The correspondence between the key points on the upper half-plane and the boundary of the unit disk are given in Table 1. The transformations are presented in Figure 4.

2.5. **Triangular domain.** Finally, we consider problem (1.1) in the complex $z-$plane when Ω is the triangle ABC with $A=(0,0)$ and B lying on the positive real axis. Here, we adopt the notation for the angles $\widehat{CAB}=\alpha$ and $\widehat{ABC}=\beta$. The problem is first mapped onto the upper half plane and subsequently onto the unit disk via transformations (2.8)-(2.9). The upper half plane is mapped onto the interior of the triangle ABC via the Schwarz–Christoffel transformation [13, 16]

$$z = \int_0^v t^{\frac{\alpha}{\pi}-1}\,(1-t)^{\frac{\beta}{\pi}-1}\,dt. \tag{2.10}$$

Clearly the point A is mapped onto the origin of the upper half plane, B onto 1 and C onto infinity. The correspondence of the vertices of the triangle ABC to the various points on the real line and the disk are presented in Table 2, while the transformations are presented in Figure 5.

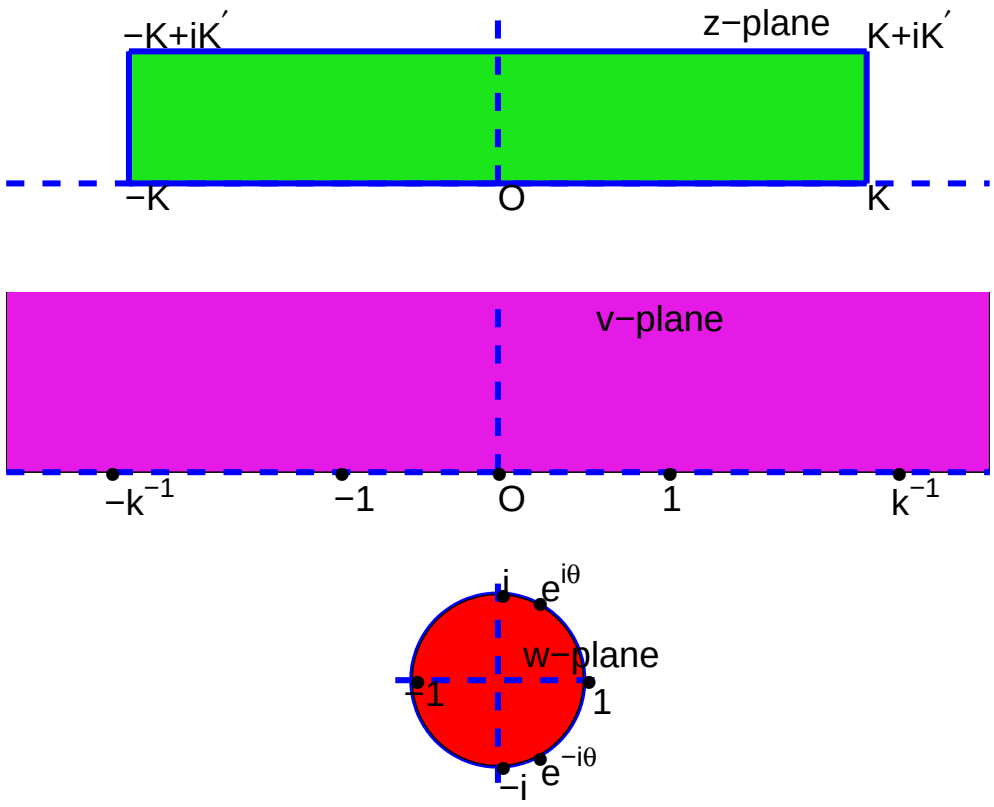

FIGURE 4. Conformal mappings from rectangle to disk.

3. METHOD OF FUNDAMENTAL SOLUTIONS

In the MFS, the solution $\tilde{u}$ of problem (1.2) is approximated by the harmonic function [15, 19]

$$u_N(\boldsymbol{c}, \boldsymbol{Q}; P) = \sum_{\ell=1}^{N} c_\ell \, \mathcal{K}(P, Q_\ell^\alpha), \qquad P \in \overline{\widetilde{\Omega}},$$

where $\boldsymbol{c} = (c_1, c_2, \ldots, c_N)^T$ and $\boldsymbol{Q}$ is a $2N-$vector containing the coordinates of the singularities (sources) Q_ℓ^α, $\ell = 1, \ldots, N$, which lie outside $\overline{\widetilde{\Omega}}$. The function $\mathcal{K}(P, Q)$ is a fundamental solution of the Laplacian given by

$$\mathcal{K}(P, Q) = -\frac{1}{2\pi} \log |P - Q|, \tag{3.1}$$

with $|P - Q|$ denoting the distance between the points P and Q. The singularities Q_ℓ^α are fixed on the boundary $\partial\widetilde{\Omega}'$ of a disk $\widetilde{\Omega}'$ concentric to the unit disk $\widetilde{\Omega}$ and defined by $\widetilde{\Omega}' = \{\boldsymbol{x} \in \mathbb{R}^2 : |\boldsymbol{x}| < R\}$, where $R > 1$. A set of collocation points $\{P_k\}_{k=1}^N$ is placed on $\partial\widetilde{\Omega}$. If $P_k = (x_{P_k}, y_{P_k})$, then we take

$$x_{P_k} = \cos \frac{2(k-1)\pi}{N}, \quad y_{P_k} = \sin \frac{2(k-1)\pi}{N}, \quad k = 1, \ldots, N.$$

If $Q_j^\alpha = \left(x_{Q_j^\alpha}, y_{Q_j^\alpha}\right)$, then

$$x_{Q_\ell^\alpha} = R \cos \frac{2(\ell - 1 + \alpha)\pi}{N}, \quad y_{Q_\ell^\alpha} = R \sin \frac{2(\ell - 1 + \alpha)\pi}{N}, \quad \ell = 1, \ldots, N, \tag{3.2}$$

where the positions of the sources differ by an angle $\dfrac{2\pi\alpha}{N}$ from the positions of the boundary points and $0 \le \alpha < 1$. In the case $\alpha \neq 0$, we thus have a *rotation* of the singularities with respect to the boundary points. This rotation is performed in order to obtain improved results when $R - 1 \ll 1$.

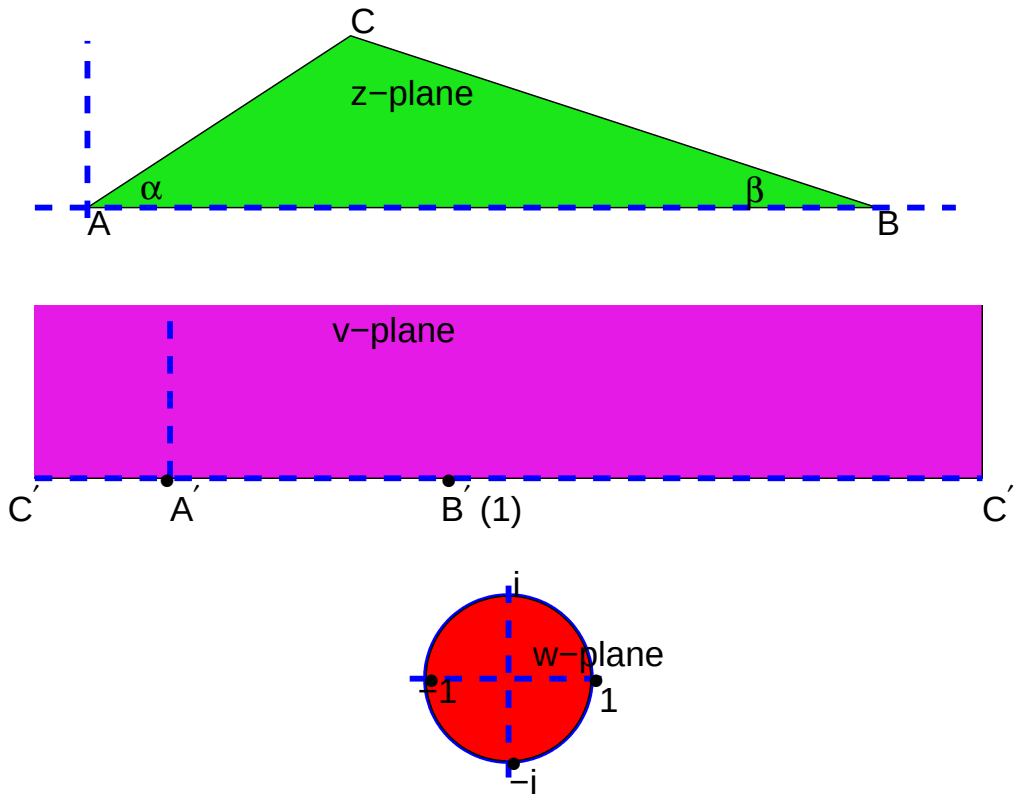

FIGURE 5. Conformal mappings from triangle to disk.

The coefficients $\boldsymbol{c}$ are determined so that the boundary condition is satisfied at the boundary points $\{P_k\}_{k=1}^N$:

$$u_N(\boldsymbol{c}, \boldsymbol{Q}; P_k) \;=\; \tilde{f}(P_k), \;\; k = 1, \ldots, N.$$

With obvious notation for $\boldsymbol{f}$, this yields a linear system of the form

$$G^\alpha \boldsymbol{c} \;=\; \boldsymbol{f}, \tag{3.3}$$

for the coefficients $\boldsymbol{c}$, where the elements of the matrix G^α are given by

$$G^\alpha_{k,\ell} = -\frac{1}{2\pi} \log |P_k - Q^\alpha_\ell|, \quad k, \ell = 1, \ldots, N.$$

Clearly, G^α is a circulant matrix and the system (3.3) can be solved efficiently using the matrix decomposition algorithm of [21, 22]. If $U^* = \frac{1}{\sqrt{N}}(\mathrm{e}^{2\pi \mathrm{i}(k-1)(\ell-1)/N})_{k,\ell=1}^N$, we premultiply system (3.3) by U to obtain $UG^\alpha U^* U\boldsymbol{c} = U\boldsymbol{f}$ or $DU\boldsymbol{c} = U\boldsymbol{f}$ or $D\hat{\boldsymbol{c}} = \hat{\boldsymbol{f}}$, where $\hat{\boldsymbol{c}} = U\boldsymbol{c}$ and $\hat{\boldsymbol{f}} = U\boldsymbol{f}$ and the matrix D is diagonal [4], with entries $\{d_j\}_{j=1}^N$. The solution is thus clearly, $\hat{c}_i = \hat{f}_i/d_i$, $i = 1, \ldots, N$. Having obtained $\hat{\boldsymbol{c}}$, we can find $\boldsymbol{c}$ from $\boldsymbol{c} = U^*\hat{\boldsymbol{c}}$. We thus have the following matrix decomposition algorithm [21, 22]:

Algorithm.

Step 1. `Compute` $\hat{\boldsymbol{f}} = U\boldsymbol{f}$.

Step 2. `Construct the diagonal matrix` D.

Step 3. `Evaluate` $\hat{\boldsymbol{c}}$.

Step 4. `Compute` $\boldsymbol{c} = U^*\hat{\boldsymbol{c}}$.

Cost. This algorithm requires $\mathcal{O}(N \log N)$ operations.

An efficient MATLAB code implementation of the method described in this section is presented in Appendix I. In it, the maximum error on the boundary is calculated in the case $f(x, y) = \mathrm{e}^{4x} \cos 4y$.

4. Numerical results

In all numerical examples, the maximum relative error on 25 uniformly distributed points (which are not collocation points) on the boundary of the unit circle was calculated for various values of N.

Example 1: Exterior of an ellipse. We first consider problem (1.1) in which Ω is the domain exterior to the ellipses defined by $\alpha = 0.1, 0.5$. The boundary condition is taken to be $f(z) = z^{-1}$ and the plots of the maximum relative error versus R are presented in Figure 8. The error in the case $\alpha = 0.1$ is much larger that in the case $\alpha = 0.5$, as the aspect ratio in the former case is much larger. In particular, in the case $\alpha = 0.1$ the ratio of the length of the major axis with respect to the length of the minor axis is 10.0333 whereas in the case $\alpha = 0.5$ it is 2.1640. Also, the conformal mapping given by (2.2) has a singularity at $z = \pm 1$ and in the case $\alpha = 0.1$, the boundary is much closer to the singular points than in the case $\alpha = 0.5$.

Example 2: Interior of an ellipse. We consider the case in which the ellipse is defined by semi-minor axis $b = 1$ and major axis $a > 1$. In (2.4) we chose $k = 3/4, 1/2$ and $1/3$ which corresponds to $a = 1.8285, 1.5249$ and 1.3785, respectively. The boundary condition is taken to be $f(z) = z^2$ and the plots of the maximum relative error versus R are presented in Figure 9. As in the case of the exterior ellipse, we observe that the error is smaller for smaller values of the aspect ratio of the ellipse (a/b). Also, the mapping function has dominant simple poles at $z = \pm \dfrac{2a\mathrm{i}}{\sqrt{a^2 - 1}}$, and as a increases the boundary approaches these poles resulting in poor convergence. (See [17].)

Example 3: Cardioid. We consider the case of a cardioid defined by $a = 1$. The boundary condition was taken to be $f(z) = z^5$. The plot of the maximum relative error versus R is presented in Figure 10 and from it we observe extremely rapid convergence of the method.

Example 4: Rectangular domain. We first consider the rectangle for which $K'/K = 1$. In this case, it follows that $k = 1/\sqrt{2}$. We considered two cases, when the boundary conditions are $f(z) = z^2$ and $f(z) = \sin z$, respectively. The plots of the maximum relative error versus R are presented in Figure 11. From these it is observed in order to obtain high accuracy, large values of N are required and the high accuracy occurs only in a small range of values of R, relatively close to the boundary. This is typical of the behaviour of the MFS for problems with boundary singularities. In Figure 12 we present $\tilde{f}(v)$ on the boundary of the disk, for $f(z) = z^2$ and $f(z) = \sin z$. From these it is clear that boundary singularities are introduced at the points corresponding to the corners of the rectangle.

We also considered the square i.e., $K'/K = 2$. From [1, Table 17.3] it follows that, in this case, $k^2 = 0.0294372515$. Again we considered the two cases when the boundary condition is $f(z) = z^2$ and $f(z) = \sin z$, respectively. In Figure 13, we present the plots of the maximum relative error versus R in the two cases. As expected the errors are considerably smaller than the errors obtained for the rectangle defined by $K'/K = 1$. In Figure 14, we present $\tilde{f}(v)$ on the boundary of the disk, for $f(z) = z^2$ and $f(z) = \sin z$ and as in the previous case, it is clear that singularities are introduced at the points corresponding to the corners of the square.

When going from the rectangle to the unit disk the conformal transformation introduces singularities at the images of at the corners of the four right angles in the sense that the first derivatives of the solution of the transformed problem becomes unbounded there. (See [14].)

Example 5: Triangular domain. We considered two cases, an equilateral triangle ($\alpha = \beta = \pi/3$) and a right–angled triangle ($\alpha = \pi/3, \beta = \pi/2$). The boundary condition is taken to be $f(z) = \sin z$ and the plots of the maximum relative error versus R are presented in Figure 15. As in the case of the rectangle, it is observed that high accuracy is only achieved for large values of N and the high accuracy occurs only in a small range of values of R, relatively close to the boundary. In Figure 16, we present $\tilde{f}(w)$ on the boundary of the disk, for the two triangles. As in the case of the rectangle, it is clear that singularities are introduced at the points corresponding to the corners of the rectangle, due to the opening–up of the angles of the triangles.

5. Doubly connected domains

In this section we extend the the ideas of Section 2 to doubly connected domains. For the existence of such conformal mappings we rely on the fact that *any doubly connected domain can be mapped conformally onto an annulus* ([29]). It should be noted that the annulus onto which the doubly–connected domain is mapped onto is one with a specific ratio of its two radii. (This ratio is called *the conformal modulus* of the domain.)

The solution of Laplace's equation in annular domains subject to Dirichlet boundary conditions can be solved very efficiently as will be explained in the sequel.

5.1. **Disk with circular hole.**

We first examine the case of a disk with a circular hole, which is not concentric to the disk. We consider the boundary value problem in the $z-$plane,

$$\Delta u = 0 \quad \text{in} \quad \Omega, \tag{5.1a}$$

$$u = f_1(z) \quad \text{on} \quad \partial\Omega_1, \quad u = f_2(z) \quad \text{on} \quad \partial\Omega_2, \tag{5.1b}$$

where Ω is a disk of radius 1 and centre $z = 0$ with a circular hole with centre $z = z_2$ and radius r_2 as shown in Figure 6. Also, $\partial\Omega_1$ outer (unit) circle while $\partial\Omega_2$ is the boundary of the hole. We assume that $r_2 < |z_2| < 1, |z_2| + r_2 < 1$, which means the hole does not cover the origin.

From [12], p.30, the conformal mapping

$$w = t\left(\frac{d\,z - s\,z_2}{d\,z - t\,z_2}\right),$$

maps Ω onto the annulus with centre the origin in the $w-$plane. The annulus has external radius 1 and internal radius $R_2 = r_2\left|\dfrac{t}{d-t}\right|$. Here $d = |z_2|$ and s and t are the (real) roots of the system of equations

$$s\,t = 1, \quad (d-s)\,(d-t) = r_2^2.$$

The inverse transformation is clearly

$$z = \frac{t\,z_2}{d}\left(\frac{w-s}{w-t}\right). \tag{5.2}$$

Therefore, via the transformation (5.2), the boundary value problem (5.1) becomes

$$\Delta\tilde{u} = 0 \quad \text{in} \quad \widetilde{\Omega}, \tag{5.3a}$$

$$\tilde{u} = \tilde{f}_1(w) \quad \text{on} \quad \partial\widetilde{\Omega}_1, \quad \tilde{u} = \tilde{f}_2(w) \quad \text{on} \quad \partial\widetilde{\Omega}_2, \tag{5.3b}$$

where $\widetilde{\Omega}$ is now an annulus in the $w-$plane, $\partial\widetilde{\Omega}_1$ is the outer (unit) circle and $\partial\widetilde{\Omega}_2$ is the inner circle of radius r_2. If the point w is a point on $\partial\widetilde{\Omega}_j$, $j = 1, 2$ in the $w-$plane corresponding to the point z in the $z-$plane, then $\tilde{f}_j(w) = f_j(z)$, $j = 1, 2$.

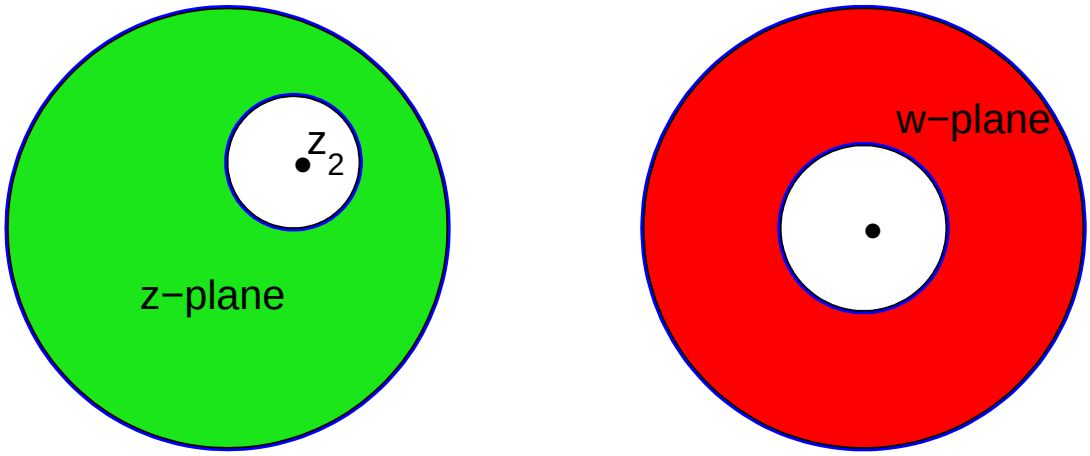

FIGURE 6. Conformal mapping from a disk with non–concentric hole to an annulus.

5.2. **Two concentric ellipses.** We next consider the case of the region between two concentric ellipses:

$$L_0 : \frac{x^2}{a_0^2} + \frac{y^2}{b_0^2} = 1 \quad \text{and} \quad L_1 : \frac{x^2}{a_1^2} + \frac{y^2}{b_1^2} = 1,$$

that is, we consider boundary value problem (5.1) where Ω is an ellipse with boundary $\partial\Omega_1 = L_0$ with a concentric elliptical hole with boundary $\partial\Omega_0 = L_1$. In the case when the ellipses are confocal, that is, $a_0^2 - b_0^2 = a_1^2 - b_1^2$, the conformal mapping [24]

$$w = \frac{z + \sqrt{z^2 - (a_0^2 - b_0^2)}}{a_0 + b_0}, \tag{5.4}$$

maps the domain Ω in the $z-$plane onto the annulus $\tilde{\Omega}$ in the $w-$plane. In this case, $\tilde{\Omega}$ has outer radius one and inner radius $R_2 = \dfrac{a_1 + b_1}{a_0 + b_0}$. The inverse transformation is given by

$$z = \frac{a_0 - b_0 + (a_0 + b_0)w^2}{2w}. \tag{5.5}$$

Thus, via transformation (5.4), boundary value problem (5.1) becomes (5.3) in the $w-$plane, as shown in Figure 7. As in the previous example, if the point w is a point on $\partial\widetilde{\Omega}_j$, $j = 1, 2$ in the $w-$plane corresponding to the point z in the $z-$plane, then $\tilde{f}_j(w) = f_j(z)$, $j = 1, 2$.

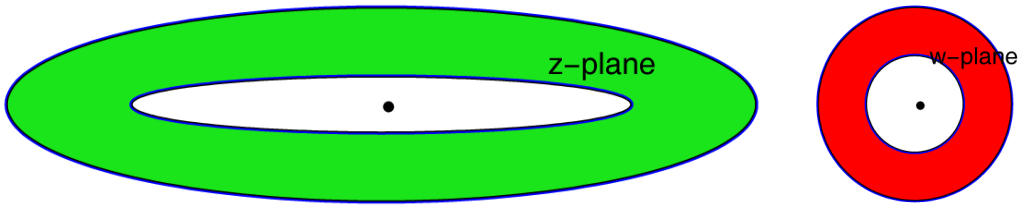

FIGURE 7. Conformal mapping from concentric ellipses to annulus.

5.3. **Method of fundamental solutions for annular domains.** In the case of the annulus, following [27], we approximate the solution $\tilde{u}$ of problem (5.3) by

$$u_N(\boldsymbol{c}_1, \boldsymbol{c}_2, \boldsymbol{Q}^1, \boldsymbol{Q}^2; P) = \sum_{\ell=1}^{N} c_{1_\ell}\, \mathcal{K}(P, Q_\ell^{1,\alpha}) + \sum_{\ell=1}^{N} c_{2_\ell}\, \mathcal{K}(P, Q_\ell^{2,\alpha}), \qquad P \in \overline{\Omega},$$

where $\boldsymbol{c}_j = (c_{j_1}, c_{j_2}, \ldots, c_{j_N})^T$, $j = 1, 2$ and $\boldsymbol{Q}^j$ are $2N-$vectors containing the coordinates of the singularities (sources) $Q_\ell^{j,\alpha}$, $\ell = 1, \ldots, N$, $j = 1, 2$, which lie outside $\overline{\widetilde{\Omega}}$. The function $\mathcal{K}(P, Q)$ is a fundamental solution of Laplace's equation given by (3.1). The singularities $Q_\ell^{1,\alpha}$ are fixed on the circle $\partial\widetilde{\Omega}_1'$ concentric to the unit circle $\partial\widetilde{\Omega}_1$ and defined by $\partial\widetilde{\Omega}' = \{\boldsymbol{x} \in \mathbb{R}^2 : |\boldsymbol{x}| = R\}$, where $R > 1$. Similarly, the singularities $Q_\ell^{2,\alpha}$ are fixed on the circle $\partial\widetilde{\Omega}_2'$ concentric to the circle $\partial\widetilde{\Omega}_2$ and defined by $\partial\widetilde{\Omega}' = \{\boldsymbol{x} \in \mathbb{R}^2 : |\boldsymbol{x}| = r\}$, where $r < R_2$.

A set of collocation points $\{P_k^j\}_{k=1}^N$, $j = 1, 2$ is placed on $\partial\widetilde{\Omega}_j$, $j = 1, 2$. If $P_k^j = (x_{P_k^j}, y_{P_k^j})$, then we take

$$x_{P_k^1} = \cos\frac{2(k-1)\pi}{N}, \quad y_{P_k^1} = \sin\frac{2(k-1)\pi}{N}, \quad k = 1, \ldots, N.$$

and

$$x_{P_k^2} = R_2 \cos\frac{2(k-1)\pi}{N}, \quad y_{P_k^2} = R_2 \sin\frac{2(k-1)\pi}{N}, \quad k = 1, \ldots, N.$$

If $Q_\ell^{j,\alpha} = \left(x_{Q_\ell^{j,\alpha}}, y_{Q_\ell^{j,\alpha}}\right)$, $j = 1, 2$, then

$$x_{Q_\ell^{1,\alpha}} = R\cos\frac{2(\ell-1+\alpha)\pi}{N}, \quad y_{Q_\ell^{1,\alpha}} = R\sin\frac{2(\ell-1+\alpha)\pi}{N}, \quad \ell = 1, \ldots, N,$$

and

$$x_{Q_\ell^{2,\alpha}} = r\cos\frac{2(\ell-1+\alpha)\pi}{N}, \quad y_{Q_\ell^{2,\alpha}} = r\sin\frac{2(\ell-1+\alpha)\pi}{N}, \quad \ell = 1, \ldots, N,$$

where α is as in (3.2). The coefficients $\boldsymbol{c}_j$, $j = 1, 2$ are determined so that the boundary conditions are satisfied at the boundary points $\{P_{j_k}\}_{k=1}^N$, $j = 1, 2$:

$$u_N(\boldsymbol{c}_1, \boldsymbol{c}_2, \boldsymbol{Q}_1, \boldsymbol{Q}_2; P_{1_k}) = \tilde{f}_1(P_{1_k}) \quad \text{and} \quad u_N(\boldsymbol{c}_1, \boldsymbol{c}_2, \boldsymbol{Q}_1, \boldsymbol{Q}_2; P_{2_k}) = \tilde{f}_2(P_{2_k}), \quad k = 1, \ldots, N. \tag{5.6}$$

With obvious notation for $\boldsymbol{f}_1$ and $\boldsymbol{f}_2$, this yields a linear system of the form

$$\left(\begin{array}{c|c} G_{11}^\alpha & G_{12}^\alpha \\ \hline G_{21}^\alpha & G_{22}^\alpha \end{array}\right) \left(\begin{array}{c} \boldsymbol{c}_1 \\ \hline \boldsymbol{c}_2 \end{array}\right) = \left(\begin{array}{c} \boldsymbol{f}_1 \\ \hline \boldsymbol{f}_2 \end{array}\right), \tag{5.7}$$

where the elements of the matrices G_{jm}^α, $j, m = 1, 2$ are given by

$$G_{jm_{k,\ell}}^\alpha = -\frac{1}{2\pi}\log|P_{j_k} - Q_{m_\ell}^\alpha|, \quad k = 1, \ldots, N \quad \ell = 1, \ldots, N, \; j, m = 1, 2, \tag{5.8}$$

Clearly, each of the matrices G_{jm}^α, $j, m = 1, 2$ is circulant and the system (5.7) can be solved efficiently as is shown in [27]. If I_2 is the identity matrix of order 2, we premultiply system (5.7) by $I_2 \otimes U$ to obtain

$$\left(\begin{array}{c|c} U & 0 \\ \hline 0 & U \end{array}\right) \left(\begin{array}{c|c} G_{11}^\alpha & G_{12}^\alpha \\ \hline G_{21}^\alpha & G_{22}^\alpha \end{array}\right) \left(\begin{array}{c|c} U^* & 0 \\ \hline 0 & U^* \end{array}\right) \left(\begin{array}{c|c} U & 0 \\ \hline 0 & U \end{array}\right) \left(\begin{array}{c} \boldsymbol{c}_1 \\ \hline \boldsymbol{c}_2 \end{array}\right) = \left(\begin{array}{c|c} U & 0 \\ \hline 0 & U \end{array}\right) \left(\begin{array}{c} \boldsymbol{f}_1 \\ \hline \boldsymbol{f}_2 \end{array}\right),$$

or

$$\left(\begin{array}{c|c} D_{11} & D_{12} \\ \hline D_{21} & D_{22} \end{array}\right) \left(\begin{array}{c} \hat{\boldsymbol{c}}_1 \\ \hline \hat{\boldsymbol{c}}_2 \end{array}\right) = \left(\begin{array}{c} \hat{\boldsymbol{f}}_1 \\ \hline \hat{\boldsymbol{f}}_2 \end{array}\right), \tag{5.9}$$

where $\hat{\boldsymbol{c}}_j = U\boldsymbol{c}_j$, $\hat{\boldsymbol{f}}_j = U\boldsymbol{f}_j$, $j = 1,2$, and each of the matrices D_{jm}, $j,m = 1,2$ is diagonal with entries d_{jm_k}, $k = 1,\dots N, j,m = 1,2$. System (5.9) is therefore equivalent to the N independent 2×2 systems

$$\left(\begin{array}{c|c} d_{11_k} & d_{12_k} \\ \hline d_{21_k} & d_{22_k} \end{array}\right)\left(\begin{array}{c} \hat{c}_{1_k} \\ \hline \hat{c}_{2_k} \end{array}\right) = \left(\begin{array}{c} \hat{f}_{1_k} \\ \hline \hat{f}_{2_k} \end{array}\right), \quad k = 1,\dots N,$$

from which we get

$$\hat{c}_{1_k} = \frac{d_{22_k}\hat{f}_{1_k} - d_{12_k}\hat{f}_{2_k}}{d_{11_k}d_{22_k} - d_{12_k}d_{22_k}} \quad \text{and} \quad \hat{c}_{2_k} = \frac{d_{11_k}\hat{f}_{2_k} - d_{21_k}\hat{f}_{2_k}}{d_{11_k}d_{22_k} - d_{12_k}d_{22_k}}, \quad k = 1,\dots N.$$

The solution is thus clearly, $\hat{c}_i = \hat{f}_i/d_i$, $i = 1,\dots,N$. Having obtained $\hat{\boldsymbol{c}}_j$, $j = 1,2$, we can find $\boldsymbol{c}$, $j = 1,2$ from $\boldsymbol{c}_j = U^*\hat{\boldsymbol{c}}_j$, $j = 1,2$. We thus have the following matrix decomposition algorithm [27]:

Algorithm

Step 1. `Compute` $\hat{\boldsymbol{f}}_j = U\boldsymbol{f}_j$, $j = 1,2$.

Step 2. `Construct the diagonal matrices` D_{jm}, $j,m = 1,2$.

Step 3. `Evaluate` $\hat{\boldsymbol{c}}_j$, $j = 1,2$.

Step 4. `Compute` $\boldsymbol{c}_j = U^*\hat{\boldsymbol{c}}_j$, $j = 1,2$.

Cost. As in the case of the disk, this algorithm can be carried out at $\mathcal{O}(N\log N)$ operations.

An efficient `MATLAB` code implementing the method described in this section is presented in Appendix II. As in the case of the unit disk, the maximum error on the boundary, when the boundary condition is $f(x,y) = \mathrm{e}^{4x}\cos 4y$, is calculated.

5.4. **Numerical results.** In the following numerical examples, the maximum relative error was calculated on 25 uniformly distributed points on each of the boundary circle of the annulus.

Example 6: Disk with circular hole. We considered the case of the unit disk with a hole with centre $z_2 = 0.3 + 0.3\mathrm{i}$ and radius $r_2 = 0.3$ which is mapped onto the annulus with external boundary the unit circle and internal boundary a circle with radius $R_2 = 0.37636943446018$ and we took the internal pseudo–boundary to be fixed with radius $r = 0.25$. The boundary condition is $f(z) = 1/(z - z_2)$. We kept the internal pseudo–boundary fixed with radius $r = R_2/2$. The plot of the maximum relative error versus R are presented in Figure 17 and from it we observe extremely rapid convergence of the method.

Example 7: Two concentric ellipses. We considered the cases when $a_0 = 9$, $b_0 = 7$, $a_1 = 6$, $b_1 = 2$ and $a_0 = 7$, $b_0 = 5$, $a_1 = 5$, $b_1 = 1$. In both cases, the annulus has inner radius $R_2 = 0.5$. The boundary condition was taken to be $f(z) = 1/z$. The plots of the maximum relative error versus R are presented in Figure 18. In the first case, the convergence is more rapid because of the smaller aspect ratio of the internal ellipse.

6. Concluding remarks

In this paper, we applied conformal mappings to harmonic Dirichlet problems in various simply– and doubly–connected domains yielding harmonic Dirichlet problems on the unit disk or an appropriate annulus. The solution of such problems using the MFS yields linear systems in which the coefficient matrices are circulant and can therefore be solved very efficiently using FFTs. Further, this removes potential sources of ill–conditioning which are inherent in the application of the MFS to simply– and doubly–connected domains. There is a potential difficulty when applying this technique to problems in non-convex polygonal domains. In these cases, the conformal transformations mapping these domains onto the disk introduce boundary singularities at the points corresponding to the non-convex

vertices. The reason for this is that these points are singularities of the Schwarz–Christoffel transformation mapping the polygon onto the upper half–plane. This means that, in such cases, more degrees of freedom are required for the accurate solution of the problem. Also, the range of the radii of the pseudo-boundaries for which accurate MFS solutions are obtained is shorter than in other problems. However, in view of the very efficient solution of the Dirichlet problem in the disk or an annulus, this may still be viewed as an improvement. In the future we intend to apply the technique described in the paper to more complex problems for which no analytical expressions for the conformal mapping exist, using numerical conformal mapping software such as `BKMPACKJ` [28], `CONFPACK` [8], `SCPACK` [26].

ACKNOWLEDGEMENTS

The authors are grateful to Professors Graeme Fairweather and Nick Papamichael for helpful discussions.

APPENDIX I

MATLAB code for the efficient solution of Dirichlet problem in the unit disk

```
function laplf(f,mp,iter,ds,alfa,m)
coe=-(1.0/(2.0*pi)); theta=2.0*pi/m; rp=1.0;
for ii=1:iter
rs=rp+ii*ds; (or alfa= (0.5*ii/(iter+1)))
ang=theta*(0:m-1); ca=cos(ang);sa=sin(ang);
ca1=cos(ang+theta*alfa);sa1=sin(ang+theta*alfa);
xp=rp*ca;yp=rp*sa;xs=rs*ca1;ys=rs*sa1; b=feval(f,xp,yp)';
dx=xp(1)*ones(1,m)-xs; dy=yp(1)*ones(1,m)-ys;
aa=.5*coe*log(dx.*dx+dy.*dy); om=exp(2.0*pi*i/m); oc=conj(om);
d=ifft(aa'); ff=fft(b)/sqrt(m); c=ff./d;
ct=real(ifft(c)/sqrt(m));
the=2.0*pi/mp; ang=the*(0:mp-1);ca=cos(ang);sa=sin(ang);
xx=rp*ca;yy=rp*sa; exa=feval(f,xx,yy);
dx=xs'*ones(1,mp)-ones(m,1)*xx; dy=ys'*ones(1,mp)-ones(m,1)*yy;
rh=.5*coe*log(dx.*dx+dy.*dy);
err=rh'*ct-exa'; a1=max(abs(err));
rt(ii,1)=rs; (or rt(ii,1)=alfa;) rt(ii,2)=a1;
end
semilogy(rt(:,1),rt(:,2),'-') (or plot(rt(:,1),rt(:,2),'-'))
function f=f1(x,y)
f=exp(4.*x).*cos(4.*y);
```

APPENDIX II

MATLAB code for the efficient solution of Dirichlet problem in an annulus

```
function lapannef(f,mp,iter,ds,alfa,m)
cf=-(1.0/(4.0*pi));theta=2.0*pi/m; rpe=1.0; rpi=0.5;
os=ones(1,m);op=ones(1,mp);ot=ones(m,1);
for ii=1:iter
rse=rpe+ii*ds;rsi=rpi/2;
ang=theta*(0:m-1); ca=cos(ang);sa=sin(ang);
ca1=cos(ang+theta*alfa);sa1=sin(ang+theta*alfa);
xpe=rpe*ca;ype=rpe*sa;xpi=rpi*ca;ypi=rpi*sa;
xse=rse*ca1;yse=rse*sa1;xsi=rsi*ca1;ysi=rsi*sa1;
be=feval(f,xpe,ype)';bi=feval(f,xpi,ypi)';
dxee=xpe(1)*os-xse;dyee=ype(1)*os-yse;aee=cf*log(dxee.*dxee+dyee.*dyee);
dxei=xpe(1)*os-xsi;dyei=ype(1)*os-ysi;aei=cf*log(dxei.*dxei+dyei.*dyei);
dxie=xpi(1)*os-xse;dyie=ypi(1)*os-yse;aie=cf*log(dxie.*dxie+dyie.*dyie);
dxii=xpi(1)*os-xsi;dyii=ypi(1)*os-ysi;aii=cf*log(dxii.*dxii+dyii.*dyii);
om=exp(2.0*pi*i/m);oc=conj(om);
dee=ifft(aee');dei=ifft(aei');die=ifft(aie');dii=ifft(aii');
ffe=fft(be)/sqrt(m);ffi=fft(bi)/sqrt(m);
ce=(dii.*ffe-dei.*ffi)./(dii.*dee-dei.*die);
ci=(-die.*ffe+dee.*ffi)./(dii.*dee-dei.*die);
cte=ifft(ce)/sqrt(m);cti=ifft(ci)/sqrt(m);
the=2.0*pi/mp;ang=the*(0:mp-1);ca=cos(ang);sa=sin(ang);
xxe=rpe*ca;yye=rpe*sa;exae=feval(f,xxe,yye);
xxi=rpi*ca;yyi=rpi*sa;exai=feval(f,xxi,yyi);
dxee=xse'*op-ot*xxe;dyee=yse'*op-ot*yye;
dxei=xsi'*op-ot*xxe;dyei=ysi'*op-ot*yye;
rhe=cf*log(dxee.*dxee+dyee.*dyee);rhi=cf*log(dxei.*dxei+dyei.*dyei);
erre=rhe'*cte+rhi'*cti-exae.';
dxie=xse'*op-ot*xxi;dyie=yse'*op-ot*yyi;
dxii=xsi'*op-ot*xxi;dyii=ysi'*op-ot*yyi;
rhe=cf*log(dxie.*dxie+dyie.*dyie);rhi=cf*log(dxii.*dxii+dyii.*dyii);
erri=rhe'*cte+rhi'*cti-exai.';
a1i=max(abs(erri));a1e=max(abs(erre));a1=max(a1i,a1e);
rt(ii,1)=rse; rt(ii,2)=a1;
end
semilogy(rt(:,1),rt(:,2),'-')
function f=f1(x,y)
f=exp(4.*x).*cos(4.*y);
```

REFERENCES

[1] M. ABRAMOWITZ AND I. E. STEGUN, *Handbook of Mathematical Functions*, Dover, New York, 1972.

[2] A. BOGOMOLNY, *Fundamental solutions method for elliptic boundary value problems*, SIAM J. Numer. Anal., **22**, 644–669, 1985.

[3] H. A. CHO, M. A. GOLBERG, A. S. MULESHKOV AND X. LI, *Trefftz methods for time dependent partial differential equations*, CMC: Computers, Materials & Continua, **1**, 1–37,2004.

[4] P. J. DAVIS, *Circulant Matrices*, John Wiley & Sons, New York-Chichester-Brisbane, 1979.

[5] G. FAIRWEATHER AND A. KARAGEORGHIS, *The method of fundamental solutions for elliptic boundary value problems*, Adv. Comput. Math., **9**, 69–95, 1998.
[6] M. A. GOLBERG AND C. S. CHEN, *The method of fundamental solutions for potential, Helmholtz and diffusion problems*, in: *Boundary Integral Methods and Mathematical Aspects*, ed. M. A. Golberg, WIT Press/Computational Mechanics Publications, Boston, 1999, pp. 103–176.
[7] P. GORZELAŃCZYK AND J. A. KOŁODZIEJ *Some remarks concerning the shape of the source contour with application of the method of fundamental solutions to elastic torsion of prismatic rods*, Eng. Anal. Bound. Elem., doi:10.1016/j.enganabound.2007.05.004, 2007.
[8] D. M. HOUGH, *User's Guide to CONFPACK*, IPS Research Report 90-11, ETH, Zürich, Switzerland, 1990.
[9] M. KATSURADA, *A mathematical study of the charge simulation method II*, J. Fac. Sci., Univ. of Tokyo, Sect. 1A, Math., **36**, 135–162, 1989.
[10] M. KATSURADA AND H. OKAMOTO, *A mathematical study of the charge simulation method I*, J. Fac. Sci., Univ. of Tokyo, Sect. 1A, Math., **35**, 507–518, 1988.
[11] E. KITA AND N. KAMIYA, *Trefftz method: an overview*, Adv. Eng. Software, **24**, 3–12, 1995.
[12] H. KOBER, *Dictionary of Conformal Representations*, Admiralty Computing Service, Department of Scientific Research and Experiment, Admiralty, London, 1944-1948.
[13] P. K. KYTHE, *Computational Conformal Mapping*, Birkhäuser, Boston, 1998.
[14] D. LEVIN, N. PAPAMICHAEL AND A. SIDERIDIS, *On the use of conformal transformations for the numerical solution of harmonic boundary value problems*, Comput. Methods Appl. Mech. Engrg., **12**, 201–218, 1977.
[15] R. MATHON AND R. L. JOHNSTON, *The approximate solution of elliptic boundary–value problems by fundamental solutions*, SIAM J. Numer. Anal., **14**, 638–650, 1977.
[16] Z. NEHARI, *Conformal Mapping*, Dover, New York, 1952.
[17] N. PAPAMICHAEL, *Dieter Gaier's contributions to numerical conformal mapping*, Comput. Methods Funct. Theory, **3**, 1–53, 2003.
[18] N. PAPAMICHAEL AND N. S. STYLIANOPOULOS, *Numerical conformal mapping onto a rectangle*, Preprint, Department of Mathematics & Statistics, University of Cyprus, 2006.
[19] Y.-S. SMYRLIS, *Applicability and applications of the method of fundamental solutions*, Tech. Report TR–03–2006, Department of Mathematics and Statistics, University of Cyprus, February 2006.
[20] Y.S. SMYRLIS, *The method of fundamental solutions: a weighted least-squares approach*, BIT, **46**, 164–193, 2006.
[21] Y.S. SMYRLIS AND A. KARAGEORGHIS, *Some aspects of the method of fundamental solutions for certain harmonic problems*, J. Sci. Comput., **16**, 341–371, 2001.
[22] Y.S. SMYRLIS AND A. KARAGEORGHIS, *Numerical analysis of the MFS for certain harmonic problems*, M2AN Math. Model. Numer. Anal., **38**, 495–517, 2004.
[23] M. R. SPIEGEL, *Complex Variables*, McGraw-Hill, New York, 1964.
[24] G. T. SYMM, *Conformal mapping of doubly-connected domains*, Numer. Math., **13**, 448–457, 1969.
[25] R. TANKELEVICH, G. FAIRWEATHER, A. KARAGEORGHIS AND Y-S. SMYRLIS, *Potential field based geometric modeling using the method of fundamental solutions*, Internat. Journal Numer. Methods in Engineering, **68**, 1257–1280, 2006.
[26] L. N. TREFETHEN, *SCPACK User's Guide*, Numerical Analysis Report 89-2, Department of Mathematics, MIT, Cambridge MA, 1989.
[27] TH. TSANGARIS, Y-S. SMYRLIS AND A. KARAGEORGHIS, *Numerical Analysis of the method of fundamental solutions for harmonic problems in annular domains*, Numer. Methods Partial Differential Equations , **21**, 507–539, 2005.
[28] M. K. WARBY, *BKMPACK User's Guide*, Technical Report, Department of Mathematics & Statistics, Brunel University, Uxbridge, UK, 1992.
[29] G-C. WEN, *Conformal Mappings and Boundary Value Problems*, Transactions of Mathematical Monographs, Vol. 106, American Mathematical Society, Providence, 1992.

DEPARTMENT OF MATHEMATICS AND STATISTICS, UNIVERSITY OF CYPRUS, 1678 NICOSIA, CYPRUS
E-mail address: andreask@ucy.ac.cy

DEPARTMENT OF MATHEMATICS AND STATISTICS, UNIVERSITY OF CYPRUS, 1678 NICOSIA, CYPRUS
E-mail address: smyrlis@ucy.ac.cy

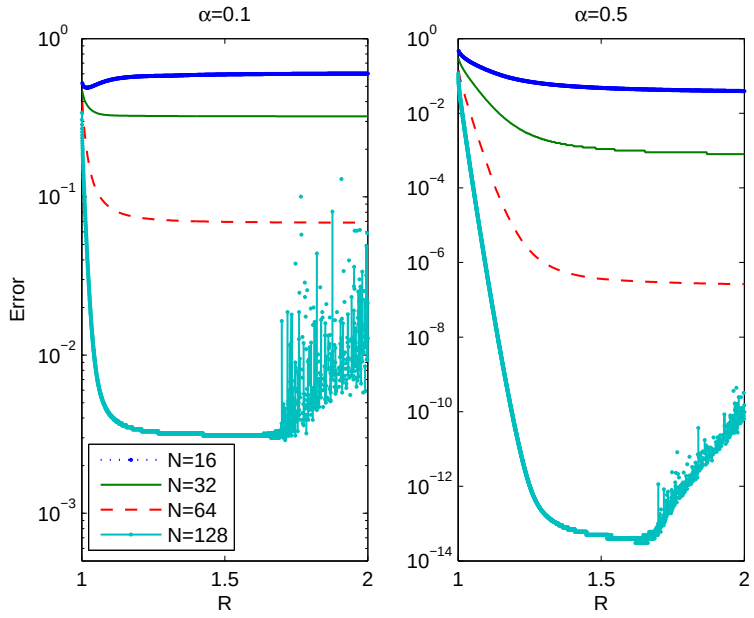

FIGURE 8. Maximum relative error versus R in Example 1, for $\alpha = 0.1, 0.5$.

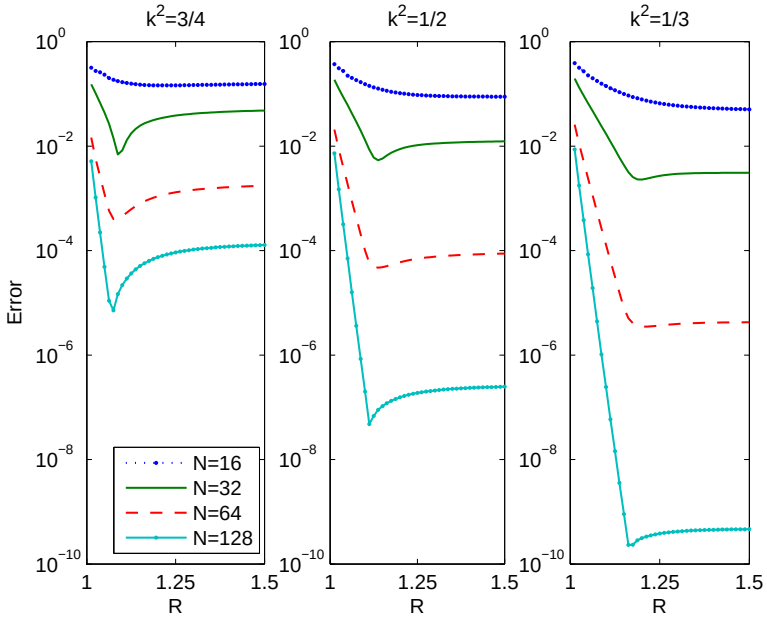

FIGURE 9. Maximum relative error versus R in Example 2, for $k = 1/2$ and $f(z) = z^2$.

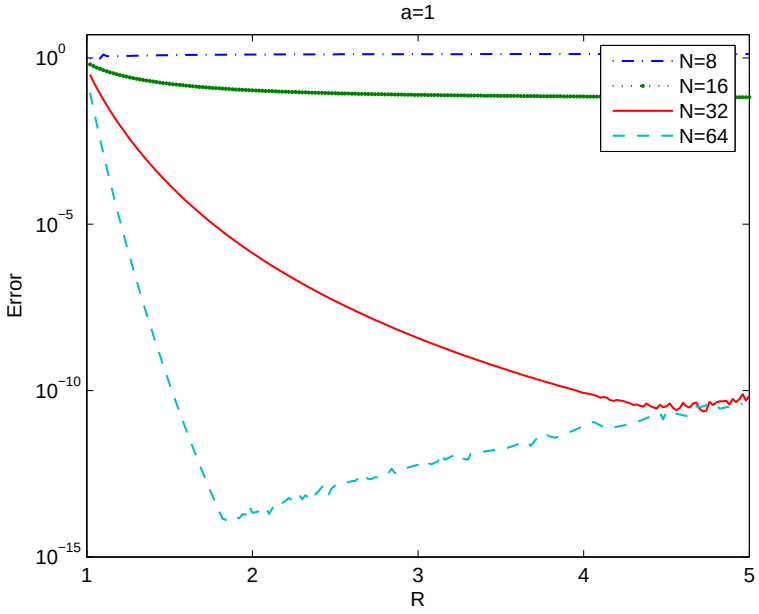

FIGURE 10. Maximum relative error versus R in Example 3, for $a = 1$ and $f(z) = z^5$.

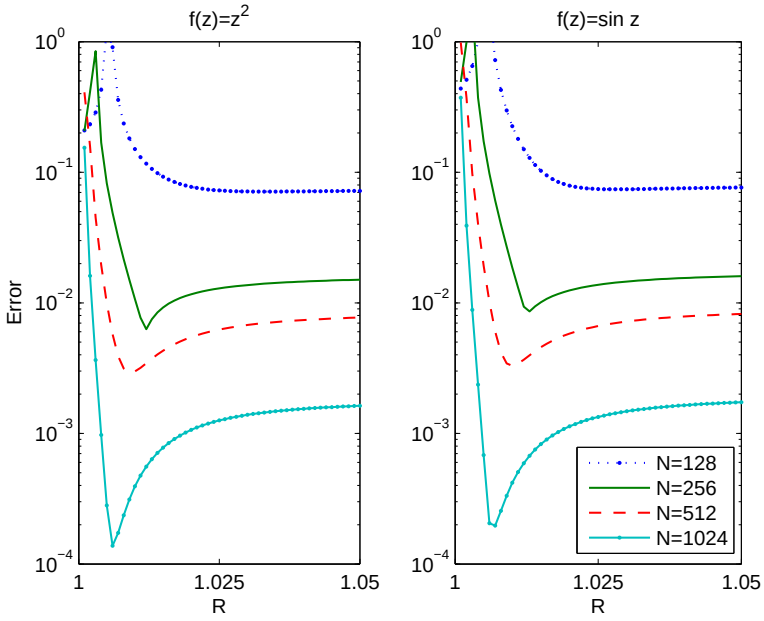

FIGURE 11. Maximum relative error versus R in Example 4, for $f(z) = z^2$ and $f(z) = \sin z$ when $K'/K = 1$

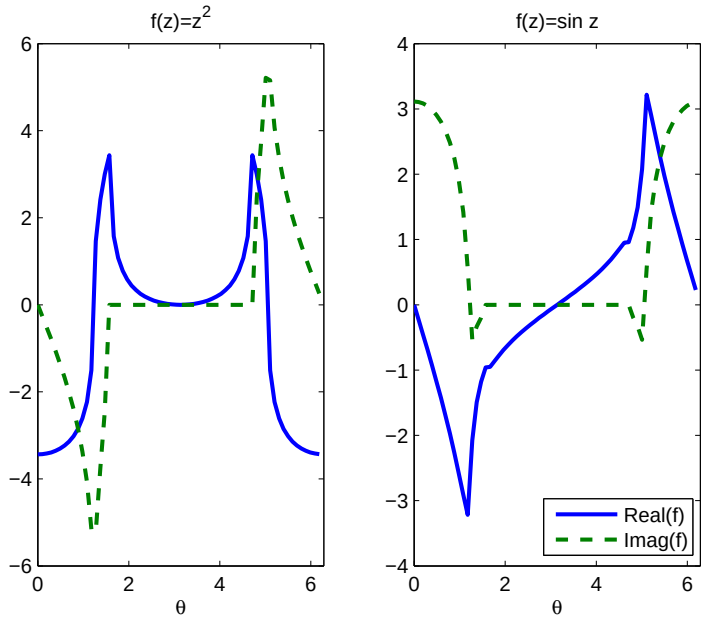

FIGURE 12. Boundary values on the boundary of the unit disk in Example 4, for $f(z) = z^2$ and $f(z) = \sin z$ when $K'/K = 1$.

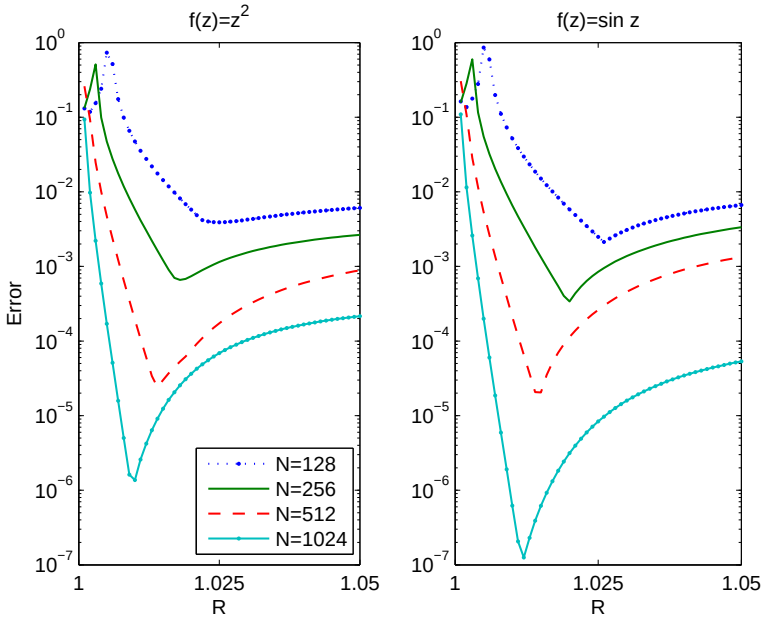

FIGURE 13. Maximum relative error versus R in Example 4, for $f(z) = z^2$ and $f(z) = \sin z$ when $K'/K = 2$.

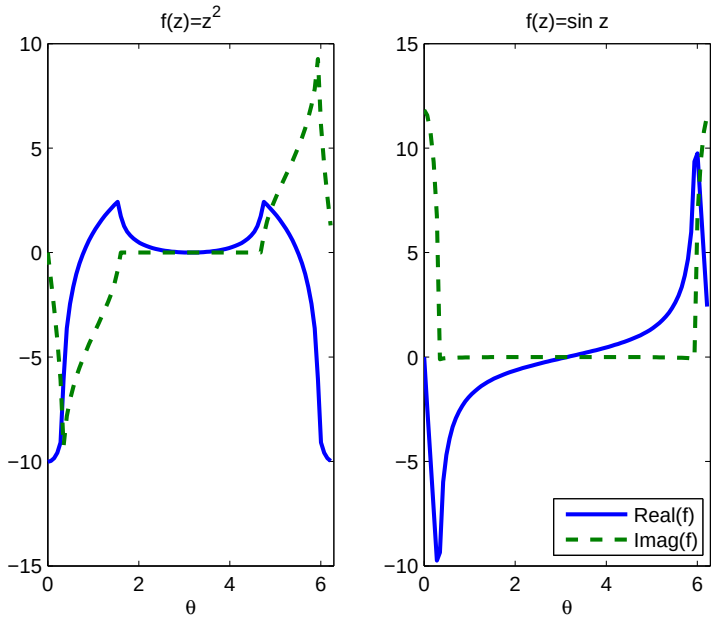

FIGURE 14. Boundary values on the boundary of the unit disk in Example 4, for $f(z) = z^2$ and $f(z) = \sin z$ when $K'/K = 2$.

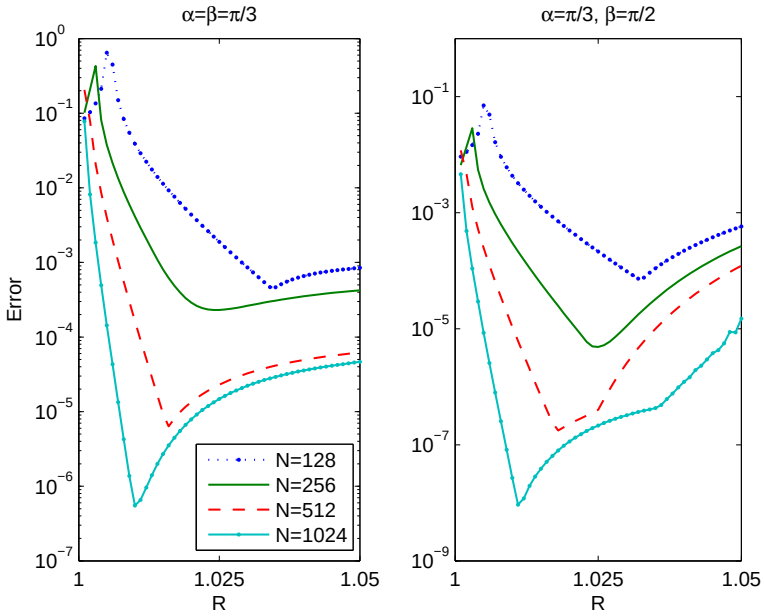

FIGURE 15. Maximum relative error versus R in Example 5, for $f(z) = \sin z$ in the cases $\alpha = \beta = \pi/3$ and $\alpha = \pi/3, \beta = \pi/2$.

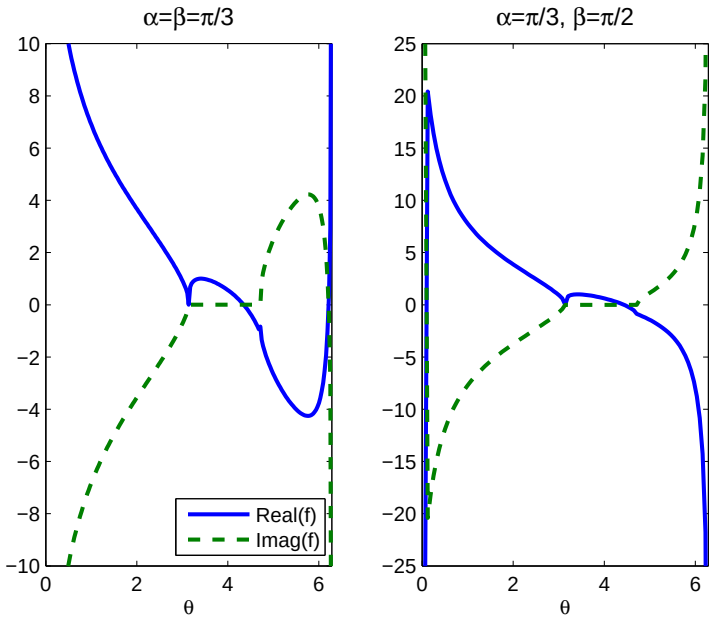

FIGURE 16. Boundary values on the boundary of the unit disk in Example 5, for $f(z) = \sin z$ in the cases $\alpha = \beta = \pi/3$ and $\alpha = \pi/3, \beta = \pi/2$.

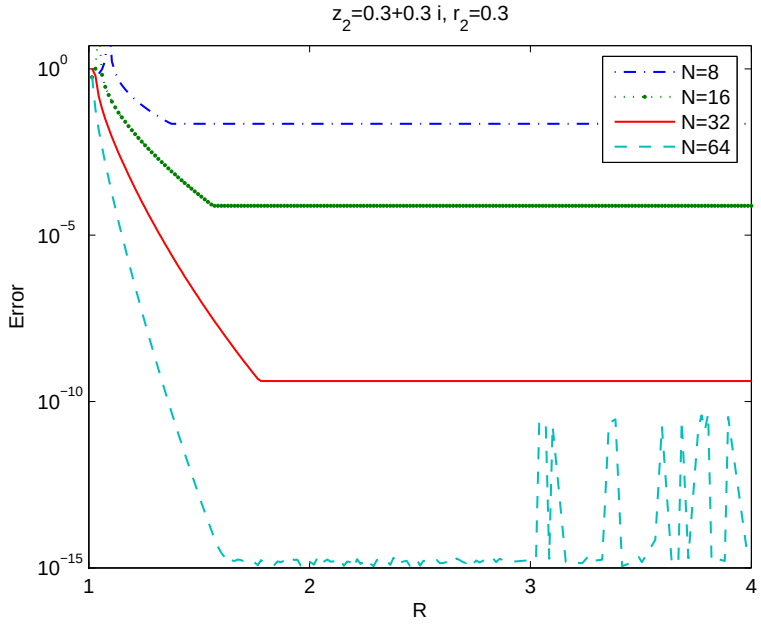

FIGURE 17. Maximum relative error versus R in Example 5, for $f(z) = 1/(z - z_2)$ in the case $z_2 = 0.3 + 0.3\mathrm{i}, r_2 = 0.3$.

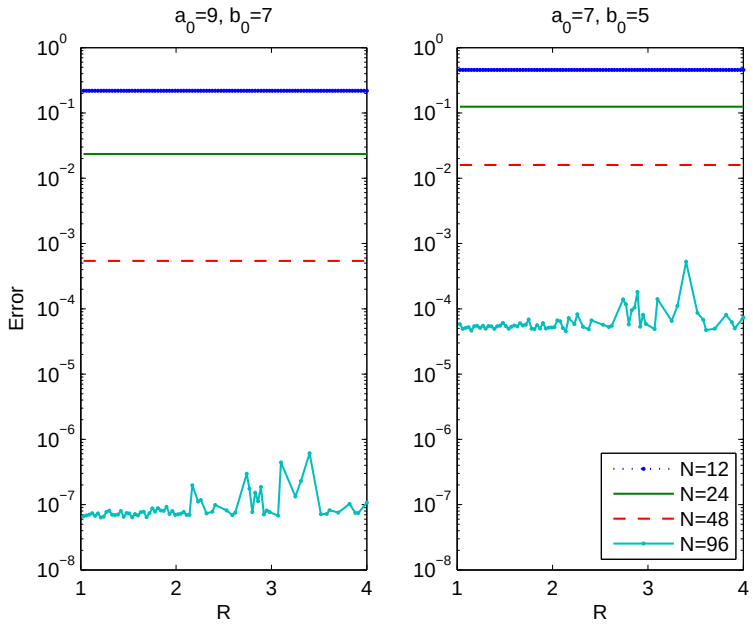

FIGURE 18. Maximum relative error versus R in Example 6, for $f(z) = 1/z$ in the cases $a_0 = 9, b_0 = 7$ and $a_0 = 7, b_0 = 5$.